



1 **Enhanced understanding of dominant drivers of**
2 **Water Yield change across China through the**
3 **improved coupled carbon and water model**

4 Huilan Shen ^{1,2}, Hanbo Yang ^{1,2,*}, Changming Li ^{1,2,3}

5 ¹ Department of Hydraulic Engineering, Tsinghua University, Beijing 100084, China

6 ² State Key Laboratory of Hydrosience and Engineering, Tsinghua University, Beijing 100084, China

7 ³ School of Civil Engineering and Transportation, State Key Laboratory of Subtropical Building and
8 Urban Science, South China University of Technology, Guangzhou 510641, China

9 * Correspondence: Hanbo Yang (yanghanbo@tsinghua.edu.cn)

10

11



Abstract: The rapid environmental changes, including climate change, escalating atmospheric CO₂ concentration ([CO₂]), and vegetation dynamics, have been significantly impacting hydrological processes. Accurately quantifying their contribution to water yield (WY) has become a significant challenge in water resource management and climate adaptation studies. Therefore, this study improved the coupled carbon and water (CCW) model integrating dynamic water use efficiency (WUE) to quantify the CO₂-physiological feedback; furthermore systematically investigated the causes for WY change during 1982-2017 in China using a scenario analysis method based on the improved CCW model. The results showed that the effects on WY from changes in climate, vegetation, and [CO₂] exhibited a significant regional variability. Climate change (especially precipitation change) emerged as the dominant driver, directly affecting over 70% of China's land area. The vegetation change was the second largest factor, especially in central China, where vegetation change led to a general decrease in runoff. The effect of the escalating [CO₂], which reduced transpiration by inducing stomatal closure, was relatively small. Spatial analysis aligned with isohyetal lines further revealed that vegetation change and [CO₂] exerted greater influence within the 400–1600 mm precipitation range. In addition, the elasticity analysis showed that the sensitivity ranking of impact factors is precipitation ($\epsilon_P = 1.55$) > [CO₂] ($\epsilon_{CO_2} = 0.55$) > NDVI ($\epsilon_{NDVI} = -0.44$) for the whole China. Historically, NDVI change has exceeded precipitation and [CO₂] impacts on runoff in some regions due to its higher relative change; however, CMIP6 SSP585 projections indicate that accelerating [CO₂] rise (2.34% yr⁻¹) will amplify its hydrological effect to a +1.29% annual WY increase by 2100, surpassing vegetation influences. This study provided theoretical support for water resource management and offered new perspectives for climate change adaptation strategies, vegetation restoration, and water resource management.

Keywords: the coupled carbon and water (CCW) model; runoff change; climate change; vegetation change; increasing atmospheric CO₂ concentrations; attribution analysis



39 **Plain language:** Climate change, rising CO₂, and vegetation dynamics are reshaping
40 global water cycle, but their impacts remain unclear. We improved the coupled carbon
41 and water model to analyze China's water yield (WY) changes (1982–2017). Our
42 results showed that climate change was the dominant driver nationally, vegetation/ CO₂
43 most affected in 400-1600 mm precipitation zones. Projections indicate CO₂ may
44 increase WY 1.3% annually by 2100, surpassing other drivers. This work informs
45 sustainable water management.



46 1 Introduction

47 The global environment has been undergoing rapid changes, impacting
48 hydrological processes through climate change, escalating atmospheric CO₂
49 concentration [CO₂], and vegetation dynamics. Notably, China has experienced a
50 visible greening trend in recent decades, prompting a heightened focus on ecological
51 and water resource concerns (Chen et al., 2019). Investigating the influence of
52 vegetation changes on runoff has thus emerged as a pivotal research area, aligning with
53 China's increasing emphasis on environmental sustainability. Understanding the
54 intricate interplay among vegetation dynamics, climate change, and [CO₂] within the
55 water cycle, particularly concerning runoff, holds significant promise for informing
56 future water resource management strategies and ecosystem preservation initiatives and
57 offering valuable insights for climate change adaptation endeavors (Ogutu et al., 2021;
58 Yang et al., 2019).

59 Climate change directly affects runoff by altering precipitation patterns,
60 temperature regimes, and radiation levels (Ban et al., 2023; Li et al., 2022). It also
61 indirectly influences runoff dynamics by altering vegetation phenology (Liu et al.,
62 2024). Vegetation, in turn, plays a key role in the hydrological cycle by influencing root
63 water uptake, canopy transpiration, rainfall interception, and soil infiltration processes
64 (Hoek Van Dijke et al., 2022; Shi et al., 2022; Yang et al., 2023; Zhang et al., 2022a).
65 Additionally, rising [CO₂] affects transpiration by influencing vegetation
66 photosynthesis, thus indirectly impacting hydrological processes (Wei et al., 2024;
67 Zhou et al., 2023). Although recent studies have attempted to separate the impacts of
68 vegetation from climate using ecohydrological models, the results remain inconsistent
69 (Fu et al., 2023; Yang et al., 2020). Some research suggested that climate change had a
70 more significant direct impact on runoff (Liu et al., 2024; Yang et al., 2021; Zhai and
71 Tao, 2017, 2021), while others highlighted the comparable or even dominant role of
72 vegetation change and [CO₂] in runoff dynamics (Li et al., 2020b; Wang et al., 2021;



73 Zhou et al., 2023). Therefore, further research is needed to disentangle the complex
74 effects of climate, vegetation, and [CO₂] change on runoff.

75 Several methods have been employed to separate the effects of climate, vegetation,
76 and [CO₂] change on runoff change, including paired catchment experiments, statistical
77 methods, and modeling approaches (Zeng et al., 2020). Given that annual water yield
78 (WY) equates to runoff through negligible soil water storage changes, these
79 methodological evaluations directly inform WY attribution frameworks (Zhang et al.,
80 2022c). The paired catchment experiment method, though classical, is limited to small-
81 scale watersheds and is less applicable to larger regions (Peng et al., 2016). Statistical
82 methods, while helpful in identifying correlations, lack a physical basis and are
83 insufficient for explaining the underlying mechanisms of runoff changes (Chen et al.,
84 2022). Modeling approaches, which are broadly categorized into conventional
85 hydrological models and ecohydrological models, provide a more systematic
86 framework for attribution analysis. Conventional hydrological models tend to focus on
87 runoff simulation and often oversimplify the effects of vegetation and [CO₂],
88 potentially underestimating their impacts on runoff (Zhai and Tao, 2021).
89 Ecohydrological models, which consider both hydrological and vegetation processes,
90 can better separate the effects of climate, vegetation, and [CO₂], but are often
91 computationally demanding and limited in their spatial applicability (Jiao et al., 2017;
92 Ma et al., 2023). Among these modeling approaches, the Budyko framework, widely
93 used to separate climate change effects on runoff, quantifies water balance through the
94 aridity index (PET/precipitation) and incorporates a catchment-specific parameter “n”
95 representing integrated land surface characteristics (e.g., vegetation, soil, topography)
96 (Zhang et al., 2022b, 2016a). However, existing studies typically attributed temporal
97 changes in “n” solely to vegetation change (Tan et al., 2024; Xue et al., 2022; Zhou et
98 al., 2023) or correlated “n” with vegetation indices (e.g., NDVI) through multivariate
99 regression (Liu et al., 2024; Tan et al., 2023)—might not accurately reflect the true
100 impact of vegetation change. This is because the approach oversimplifies the role of “n”



101 by conflating vegetation effects with confounding factors (e.g., CO₂-induced stomatal
102 adjustments, and climate change), as regression-based methods inherently fail to
103 disentangle covarying drivers, thereby obscuring whether “n” changes originate from
104 vegetation dynamics, CO₂-physiological feedbacks, or multi-factor synergies (Gan et
105 al., 2021). While some studies incorporated [CO₂] effects via PET adjustments instead
106 of actual evapotranspiration, this indirect approach conflates CO₂-driven PET changes
107 with other meteorological drivers (e.g., radiation, wind) and propagates parameter
108 uncertainties (e.g., “n”), obscuring [CO₂]’s independent impact on runoff (Liu et al.,
109 2024).

110 The coupled carbon and water (CCW) model integrates hydrological and
111 ecological processes by mechanistically linking vegetation dynamics to water and
112 carbon fluxes through remote sensing-driven parameterization (Li et al., 2024b; Zhang
113 et al., 2021b, 2022c). Unlike the Budyko framework’s empirical parameter “n”—which
114 conflates vegetation effects with unaccounted catchment characteristics—CCW
115 explicitly resolves vegetation impacts through two distinct pathways: (1) structural
116 effects—quantified by NDVI-modulated canopy absorption of photosynthetically
117 active radiation (FPAR) that captures changes in energy partitioning due to vegetation
118 greening; and (2) physiological adjustments—represented by biome-specific variations
119 in underlying water-use efficiency (UWUE) and vapor pressure deficit (VPD)-
120 mediated regulation of evapotranspiration (ET). In the model, GPP is estimated from
121 light-use efficiency theory ($\epsilon_{\text{pot}} \times \text{FPAR} \times \text{PAR} \times R_s \times T_s \times W_s$), and ET is
122 mechanistically coupled to GPP via UWUE—a physiologically grounded parameter
123 representing ecosystem-level carbon–water trade-offs, calibrated against global
124 FLUXNET observations (Zhang et al., 2016b), which encapsulates ecosystem-level
125 carbon–water trade-offs. By contrast, Budyko’s empirical “n” aggregates these distinct
126 vegetation controls into a single catchment-scale parameter, obscuring their individual
127 hydrological impacts.



128 Nevertheless, the original CCW model, while robust in capturing vegetation-
129 climate interactions, does not account for CO₂-induced physiological changes,
130 specifically long-term enhancements in water-use efficiency (WUE) resulting from
131 elevated [CO₂] (Adams et al., 2020; Li et al., 2023). This omission limits its ability to
132 isolate [CO₂] fertilization effects from climate and LULC (land use and land cover)
133 changes, a gap particularly problematic in regions like China, where CO₂-driven WUE
134 improvements may offset or amplify vegetation greening impacts on runoff.

135 Therefore, we aim to improve the CCW model by incorporating dynamic WUE
136 responses to [CO₂], building on the biome-specific UWUE framework. Furthermore,
137 by integrating CO₂-dependent WUE adjustments into the ET-GPP coupling, our
138 improved model explicitly partitions runoff changes into three causal drivers: (1)
139 climate change (eg. precipitation, temperature, and so on), (2) vegetation structural
140 changes (NDVI, and land use and land cover (LULC)), and (3) CO₂-physiological
141 effects (stomatal optimization).

142 **2 Methods and Data**

143 **2.1 Data sources and processing**

144 Four main datasets were employed in the improved CCW model: vegetation data
145 (NDVI), climate data (precipitation, temperature, shortwave radiation, vapor pressure
146 deficit, and atmospheric pressure), land use and land cover (LULC), and [CO₂]. The
147 monthly NDVI dataset used in this study (Table 1) was derived from a daily 0.05° gap-
148 free NDVI dataset in China (<https://doi.org/10.6084/m9.figshare.c.7002225.v1>) (Li et
149 al., 2024a), which was developed from the NOAA's daily NDVI dataset, applying
150 effective data recognition and spatiotemporal gap-filling techniques. The dataset spans
151 1981–2023 and provides a spatial resolution of 0.05°, and we used bilinear interpolation
152 to generate the dataset with a spatial resolution of 0.1°.

153 Climate data (Table 1), including precipitation, air temperature, surface downward
154 shortwave radiation, relative humidity, and atmospheric pressure, were sourced from



155 the China Meteorological Forcing Dataset (CMFD) at the National Tibetan Plateau
156 Data Center (TPDC) of the Institute of Tibetan Plateau Research, Chinese Academy of
157 Sciences (He et al., 2020). The dataset spans 1979–2018 and provides a spatial
158 resolution of 0.1° and temporal resolutions at 3-hour, daily, monthly, and annual scales.
159 As the dataset did not provide vapor pressure deficit (VPD), we calculated VPD using
160 the method from Howell and Dusek (1995), based on atmospheric pressure, temperature,
161 and relative humidity.

162 LULC data (Table 1) were obtained from the Zhang et al. (2024) global dataset,
163 which provides consistent multi-temporal global LULC maps at 30 m spatial resolution
164 for 1985–2022. The dataset includes 35 fine-resolution LULC types. For the purposes
165 of this study, and to facilitate LULC change analysis, we merged these 35 LULC types
166 into 17 types using the IGBP classification, based on the method by Yang et al. (2017).
167 Four primary LULC types—cropland, forest, grassland, and bare land—were
168 determined following the method described by Mu et al. (2013). The data were
169 resampled to the 0.1° spatial resolution, ensuring compatibility for modeling within the
170 modified CCW framework.

171 $[\text{CO}_2]$ data were sourced from the Mauna Loa Observatory (MLO), Hawaii (20°N ,
172 156°W) (<http://cdiac.esd.ornl.gov/ftp/trends/co2/maunaloa.co2>), with yearly
173 observations used to represent national $[\text{CO}_2]$ levels due to the minimal spatial variation
174 in $[\text{CO}_2]$ across China (Table 1). These datasets were then used to drive the improved
175 CCW model.

176 In this study, the hydrological data for model validation from 145 hydrological
177 stations (Fig. 1), each with at least 15 years of continuous data since 1982, was collected
178 from the Hydrological Bureau of the Ministry of Water Resources of China
179 (<https://www.mwr.gov.cn/english/>). Annual runoff data were calculated from the daily
180 runoff and the catchment area controlled by each hydrological station.

181 **Table 1.** Hydrology, climate, and vegetation data for the improved CCW model



Dataset	Original Resolution (spatial/temporal)	Period	Reference
NDVI	0.05° × 0.05° (daily)	1981 - 2023	(Li et al., 2024a)
Landcover	30m×30m (5-year)	1985 - 2022	(Zhang et al., 2024)
Climate	0.1° × 0.1° (monthly)	1979 - 2018	(He et al., 2020)
[CO ₂]	yearly	1959 - 2023	Mauna Loa Observatory, Hawaii
Streamflow	daily	1982 - 1995 (or later)	On-site streamflow records and the regional flow summary reports of government

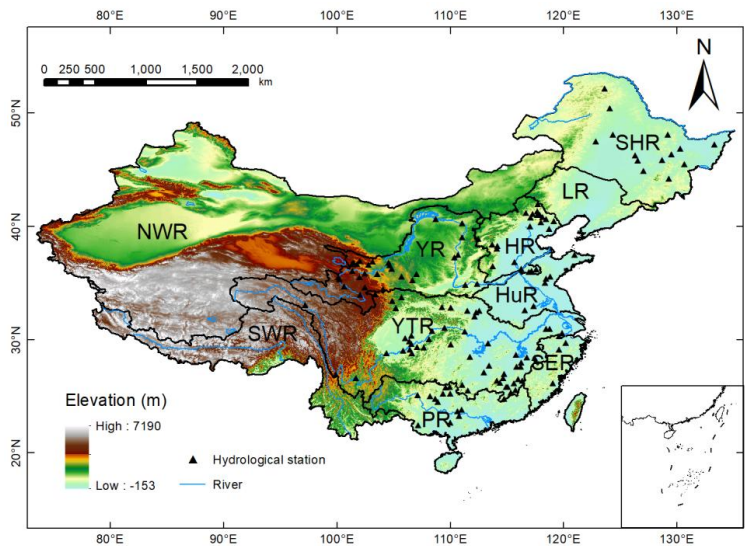


Figure 1. The geographic location and topography of the study area, where the black triangles mark the location of the hydrological gauging stations for model evaluation. Ten river basins considered in this study are: Songhua River basin (SHR), Liao River basin (LR), Hai River basin (HR), Huai River basin (HuR), Yangtze River basin (YZR), Yellow River basin (YR), Pearl River basin (PR), Southeast Rivers (SER), Southwest Rivers (SWR) and Northwest Rivers (NWR).

2.2 The improved CCW model

The original Coupled Carbon and Water (CCW) model (Zhang et al., 2016b) is a data-driven, remote sensing-based model that effectively integrates carbon and water dynamics to estimate monthly gross primary productivity (GPP) and evapotranspiration (ET). This model, which is particularly carbon-centric, derives ET from GPP constrained by underlying water-use efficiency (UWUE) parameters, which were calibrated using global FLUXNET data (Zhang et al., 2016b; Zhou et al., 2014). Despite



196 its simpler structure, the CCW model achieves accuracy comparable to more complex
197 process-based models in ET estimation. The essential components of the CCW model
198 are represented as:

$$199 \quad GPP = APAR \times \varepsilon = PAR \times FPAR \times \varepsilon_{pot} \times R_s \times T_s \times W_s \quad (1)$$

200 where APAR is the absorbed photosynthetically active radiation (MJ m^{-2}), which is
201 calculated as the product of incident photosynthetically active radiation (PAR) and the
202 fraction of PAR absorbed by vegetation (FPAR), and PAR is typically assumed to be
203 45% of the total shortwave radiation (Running et al., 2000); FPAR is determined by the
204 normalized difference vegetation index (NDVI) (Sims et al., 2005); ε is the realized
205 light-use efficiency (g C MJ^{-1}), which is calculated by multiplying the potential light-
206 use efficiency (ε_{pot}) and environmental scalars for diffuse radiation (R_s), temperature
207 (T_s), and moisture stress (W_s). This formulation ensures that GPP estimates reflect the
208 influence of radiation, temperature, and moisture limitations on photosynthetic activity.

209 In this study, we improve the CCW model by incorporating dynamic water use
210 efficiency (WUE) instead of static UWUE. This enhancement addresses the limitations
211 of the original model, particularly its inability to adapt to environmental changes such
212 as varying $[\text{CO}_2]$ and vapor pressure deficit (VPD). WUE's estimation method is
213 estimated using the WEC (Water Efficiency and Carbon) equation proposed by Cheng
214 et al. (2017). The final formula for calculating WUE is:

$$215 \quad WUE = \frac{C_a \times P_a}{1.6(VPD + g_1 \sqrt{VPD})} [1 - \exp(-k * LAI)](1 - f_i) \quad (2)$$

216 where C_a is atmospheric CO_2 concentration ($\text{mol}(\text{CO}_2) \text{ mol}^{-1}(\text{air})$); P_a is atmospheric
217 pressure (kPa); VPD is vapor pressure deficit (kPa); g_1 is an empirical parameter of the
218 Ball stomatal conductance model; k is the radiation extinction coefficient, typically set
219 at 0.6, describing how light is absorbed by the canopy; LAI is the leaf area index; and
220 f_i is a factor representing nonproductive water use (such as evaporation from soil and
221 canopy interception). This equation provides a dynamic estimate of WUE, considering
222 the effects of environmental factors like VPD, CO_2 concentration, atmospheric pressure,



223 and canopy structure (LAI). The factor $1 - \exp(-k \times \text{LAI})$ accounts for light interception
224 by the canopy.

225 In order to ensure the consistency of NDVI and LAI trends, we calculated LAI
226 using NDVI (Gutman and Ignatov, 1998) instead of LAI dataset:

$$227 \quad \begin{cases} LAI = -2 \ln(1 - f_{NDVI}) \\ f_{NDVI} = \frac{NDVI - NDVI_0}{NDVI_1 - NDVI_0} \end{cases} \quad (3)$$

228 where $NDVI_0 = 0.04$, $NDVI_1 = 0.52$

229 Evapotranspiration (ET) is then calculated as the ratio of GPP to WUE:

$$230 \quad ET = \frac{GPP}{WUE} \quad (4)$$

231 This modification allows the model to estimate ET using dynamic WUE, replacing the
232 static UWUE from the original model. The dynamic nature of WUE enhances the
233 model's ability to simulate ecosystem water use across different environmental
234 conditions and vegetation types.

235 Finally, the water yield (WY) is calculated as the difference between precipitation
236 (P) and ET:

$$237 \quad WY = P - ET \quad (5)$$

238 On an annual scale, WY is assumed to be approximately equal to runoff, as
239 changes in soil water storage over long periods (one year or longer) are considered
240 negligible. Thus, the attribution of WY can also be considered as the attribution of
241 runoff.

242 **2.3 Attribution analysis framework**

243 To explore the combined and individual effects of climate, vegetation, and $[\text{CO}_2]$
244 change on water yield (WY), four scenarios were designed based on data from 1982 to
245 2017 (Table 2). Scenario 1 (Actual) aimed to validate the improved CCW model and
246 estimate the combined effects of climate, vegetation, and $[\text{CO}_2]$ change on WY by



247 allowing all variables to vary from 1982 to 2017. Scenario 2 (Vegetation Change)
248 focused on estimating the direct effects of vegetation change on WY by allowing
249 vegetation variables (NDVI and LULC) to vary while keeping climate and [CO₂] fixed
250 at 1982 levels. In this case, the trend in WY obtained reflects the impact of vegetation
251 change alone. Scenario 3 (Climate Change) aimed to estimate the direct effects of
252 climate change on WY by allowing climate variables (precipitation, temperature,
253 relative humidity, solar radiation, and atmospheric pressure) to change, while fixing
254 vegetation and [CO₂] at 1982 levels. This scenario helps isolate the effects of climate
255 change on WY. Scenario 4 ([CO₂] Change) was designed to estimate the direct effects
256 of [CO₂] change on WY by varying [CO₂] levels from 1982 to 2017, while climate and
257 vegetation variables were fixed at 1982 levels. The resulting WY trend reflects the
258 impact of [CO₂] change alone.

259 **Table 2.** Scenario designs in the improved CCW model for WY attribution. LULC: Land use
260 and land cover types; NDVI: Normalized difference vegetation index; TMP: Temperature;
261 SRAD: Shortwave radiation; VPD: Vapor pressure deficit.

Scenarios	Vegetation		Climate					CO ₂	Purposes
	LULC	NDVI	P	T	RH	Srad	Pa	CO ₂	
S1 (baseline)	▲	▲	▲	▲	▲	▲	▲	▲	Validating the improved CCW model and estimating the combined effects of climate, vegetation, and CO ₂ change.
S2 (vegetation)	▲	▲	△	△	△	△	△	△	Estimating the direct effects of vegetation change.
S3 (climate)	△	△	▲	▲	▲	▲	▲	△	Estimating the direct effects of climate change.



S4
(CO₂) △ △ △ △ △ △ △ ▲ Estimating the
direct effects of
CO₂ change.

262 Note: The symbol “▲” denotes a changing input variable over time, whereas the symbol “△”
263 represents a fixed input variable at the level of the initial year (1982).

264 The relative contributions of climate, vegetation, and [CO₂] to changes in WY
265 were calculated using the following formula:

$$266 \quad \begin{cases} RC_{vegetation} = \frac{trend_{vegetation}}{|trend_{vegetation}| + |trend_{climate}| + |trend_{CO_2}|} \times 100\% \\ RC_{climate} = \frac{trend_{climate}}{|trend_{vegetation}| + |trend_{climate}| + |trend_{CO_2}|} \times 100\% \\ RC_{CO_2} = \frac{trend_{CO_2}}{|trend_{vegetation}| + |trend_{climate}| + |trend_{CO_2}|} \times 100\% \end{cases} \quad (6)$$

267 where $trend_{vegetation}$, $trend_{climate}$, and $trend_{CO_2}$ represent the changes in water
268 yield (WY) resulting from vegetation, climate, and [CO₂] changes, respectively, as
269 calculated in each scenario; the relative contributions ($RC_{vegetation}$, $RC_{climate}$, and
270 RC_{CO_2}) are expressed as percentages, indicating the proportion of each factor's
271 influence on the overall changes in WY.

272 At each grid point, the absolute values of the relative contributions of each factor
273 (vegetation, climate, and [CO₂]) are compared. For each grid point, we identify the
274 most significant contributor to water yield (WY) changes by comparing the relative
275 contributions of each factor. If the absolute values of the relative contributions of two
276 factors do not exceed 5%, then these two factors are considered joint significant
277 contributors to the changes in WY at that grid point (Ma et al., 2024; Saltelli et al.,
278 2007). This approach helps to highlight areas where the impacts of multiple factors are
279 closely intertwined and both play a critical role in influencing water yield, suggesting
280 that their combined effects are comparable in magnitude. In these cases, the relative
281 contribution of each factor is not significantly stronger than the other, indicating that
282 their combined influence on WY is equally important at the local scale.



283 The scenario analysis previously conducted revealed the relative contributions of
284 climate, vegetation, and [CO₂] to WY changes. However, these contributions arise from
285 both the intrinsic rate of change of each factor and the sensitivity of runoff to those
286 changes (the elasticity coefficient) (Yang and Yang, 2011). To gain a deeper
287 understanding of the changes in WY, we employ elasticity coefficients to quantify its
288 sensitivity to individual factor. We specifically focused on precipitation because,
289 despite not always having the highest sensitivity, it is integral to the hydrological cycle
290 and essential for assessing water yield (WY) under various climate change scenarios
291 (Liu et al., 2017). The elasticity of runoff refers to the variation in runoff depth resulting
292 from a 1% increase in each climatic variable (Xu et al., 2014). The absolute value of
293 elasticity reflects the sensitivity of runoff to various influencing factors. In other
294 methods, elasticity coefficients are typically calculated using an analytical expression
295 based on instantaneous changes in runoff corresponding to variations in a given factor
296 in a specific year (Fu et al., 2023; Liu et al., 2017; Yang and Yang, 2012). However, in
297 our study, we applied scenario-based analysis over the period of 1982 to 2017. This
298 extended temporal window allowed us to better account for the long-term effects and
299 interactions of multiple factors influencing WY. So we vary each factor (precipitation,
300 NDVI, and [CO₂]) by 1% relative to the baseline scenario S1 across the entire 1982-
301 2017 period. We then calculated the annual average runoff values from the adjusted
302 sequence and compared them with the average original baseline runoff values. The
303 difference between these two values, divided by the average baseline runoff value, gave
304 us the runoff change rate:

$$\frac{\Delta R_x}{R_x} = \frac{WY_{mean_x} - WY_{mean_x}}{WY_{mean_x}} \quad (7)$$

306 Mathematically, the elasticity coefficient is defined as the runoff change rate
307 divided by 1%, and the formula is as follows:

$$\varepsilon_x = \frac{\frac{\Delta R_x}{R_x}}{\frac{\Delta x}{x}} = \frac{\frac{\Delta R_x}{R_x}}{1\%} \quad (8)$$



309 Generally, while the scenario analysis above has identified which factors are most
310 influential based on their relative contributions, the elasticity coefficients allow us to
311 explain why these factors are critical by demonstrating their respective impacts on WY
312 through sensitivity analysis. This dual approach—combining both the changes in the
313 factors and their elasticities—provides a more comprehensive understanding of the
314 drivers behind the observed changes in WY, ensuring that the results of the scenario
315 analysis are both meaningful and robust.

316 **3 Results**

317 **3.1 Changes in hydrometeorological variables**

318 Fig. 2 demonstrates the trends of annual precipitation, air temperature, relative
319 humidity, atmospheric pressure, solar radiation, and NDVI across China during 1982-
320 2017. Annual precipitation change exhibited a clear spatial distribution pattern,
321 specifically decreases in central China, including the middle reaches of the Yellow
322 River and the Yangtze River basins, and increases in the northwest and southeast. Air
323 temperature exhibited a consistent warming trend across China. In contrast, relative
324 humidity generally decreased across most China. Atmospheric pressure remained
325 relatively stable. Regarding solar radiation, decreases were in northern China, while an
326 increase was in southern regions. The decreasing solar radiation in northern China is
327 likely due to increased aerosol concentrations (Liang et al., 2024). NDVI showed a
328 significant increasing trend, which indicates an overall enhancement in vegetation
329 growth across China. This trend was especially prominent in central and eastern regions,
330 including the Yellow River Basin and the Yangtze River Basin. In these regions, LULC
331 changes, such as afforestation and agricultural practices, likely contributed to the
332 observed increases in NDVI (Chen et al., 2019).

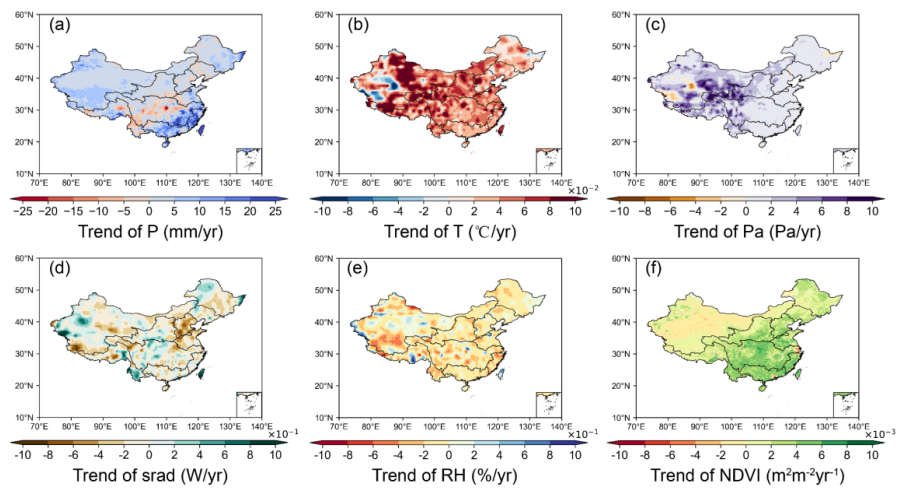


Figure 2. Spatial patterns of trends in annual climatic and vegetation variables during 1982–2017. (a) precipitation (mm/yr); (b) air temperature ($^{\circ}\text{C}/\text{yr}$); (c) Atmospheric pressure (Pa/yr); (d) shortwave radiation ($\text{W}/\text{m}^2/\text{yr}$); (e) relative humidity ($\%/ \text{yr}$); (f) NDVI (yr^{-1}).

Significant changes in land use and land cover (LULC) occurred in China during 1982–2017, as illustrated in Fig. 3. Although the overall percentage distribution of major land cover types, namely grasslands, forests, croplands, and bare lands, remained relatively stable, these four categories dominated the landscape, with most changes concentrated within them. Notably, the transitions among these categories were characterized by mutual conversions, particularly from bare land to grasslands (Fig. 3). Spatially, the changes exhibited distinct regional patterns. In southern China, LULC changes were mainly characterized by the conversion of land to forests and grasslands. In contrast, the northeastern regions exhibited more complex transformations, with some areas shifting to bare land and croplands (Fig. 3).

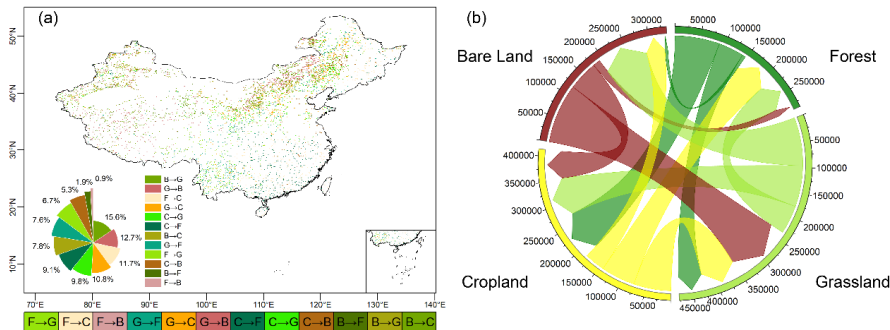


Figure 3. Land use and land cover (LULC) changes from 1982 to 2017. (a) Spatial pattern distribution of LULC change; (b) Chord diagram of LULC conversion flows (unit: km²), where directional arrows represent transitions between land types (originating type → current type), with chord widths proportional to the converted areas. The figure illustrates the converted areas and does not include the unchanged regions.

3.2 Performance of the improved CCW model

As shown in Fig. 4a, the observed annual water yield (WY) and the simulated annual WY by the improved CCW model showed strong linear correlations ($R^2 = 0.7$), with the regression line slope being 1.45, R^2 being 0.7, and RMSE being 12.49 mm/year. It indicates that the model provides a reliable representation of the observed trends.

The estimated annual WY trends had distinct spatial patterns (Fig. 4b), which closely aligned with that of precipitation. Specifically, decrease trends in WY occurred in the central regions of the Yellow River Basin and the middle section of the Yangtze River Basin, while increase trends were found in other regions, with the southeast exhibiting the highest rate of increase.

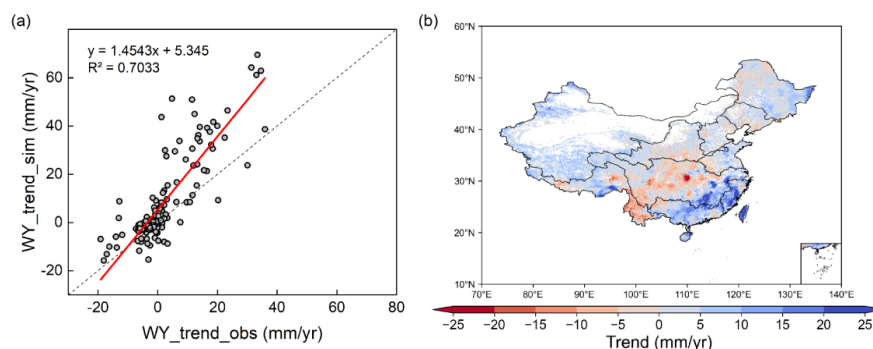
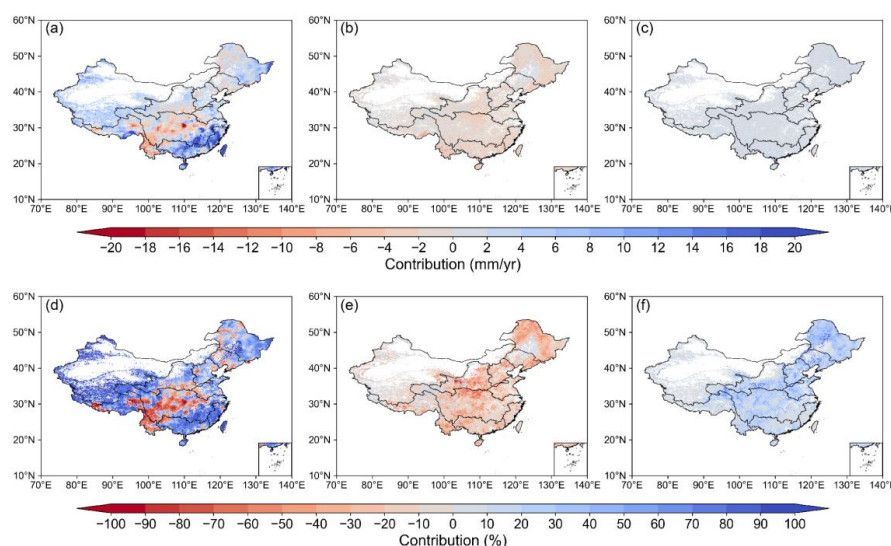


Figure 4. (a) Validation of simulated WY trend using the improved CCW model; (b) Spatial distribution of WY trends under scenario S1(actual situation) during 1982–2017.

3.3 Attribution analysis of annual WY changes

Fig. 5 shows the distribution of WY changes caused by climate, vegetation, and [CO₂] changes, integrating both absolute magnitude (Fig. 5a-c) and relative dominance (Fig. 5d-f) of their contributions. Climate-driven WY changes exhibited marked spatial heterogeneity, with absolute increases exceeding 15 mm/yr in southeastern China (Fig. 5a), corresponding to 60-90% relative contributions (Fig. 5d). Central basins showed contrasting declines of 0-6 mm/yr under climate forcing, while northeastern transitional zones displayed mixed positive/negative absolute changes (Fig. 5a) despite maintaining 40-70% relative climate dominance (Fig. 5d). This spatial heterogeneity aligned with precipitation change patterns (Fig. 2a).



376

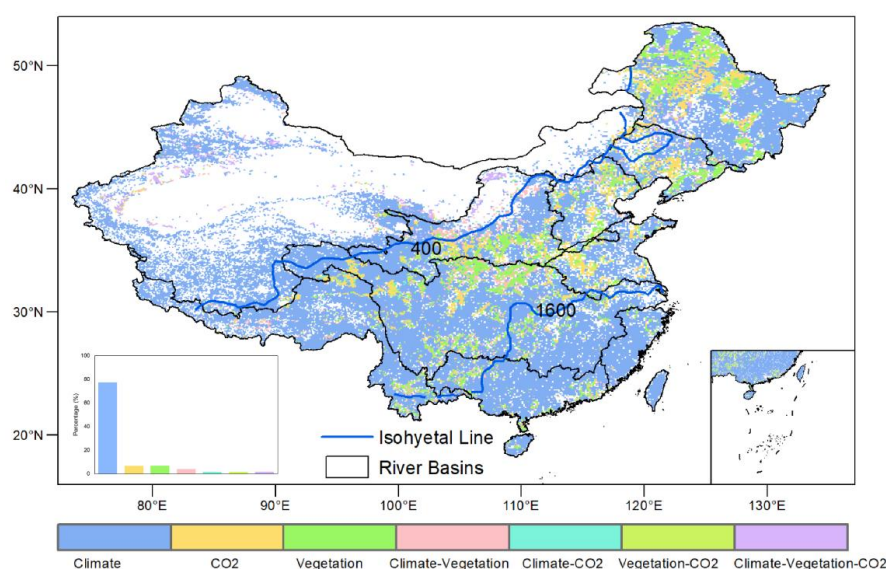
377 **Figure 5.** The absolute contributions of (a) climate, (b) vegetation, and (c) [CO₂], and the
378 relative contributions of (d) climate, (e) vegetation, and (f) [CO₂] to changes in WY trends for
379 1982-2017.

380 Vegetation-mediated WY reductions reached 0-6 mm/yr (Fig. 5b), accompanied
381 by 0-60% relative contributions (Fig. 5e). These effects originated from enhanced
382 evapotranspiration through land-use changes and NDVI-based greening, particularly
383 pronounced in central China. Specific regions in the Yangtze, Yellow, and northeastern
384 rivers showed vegetation-driven relative contributions reaching 40-60% (Fig. 5e). [CO₂]
385 effects generated limited direct absolute impacts (<5 mm/yr, Fig. 5c) but exerted 10-
386 40% relative influences (Fig. 5f) through stomatal closure mechanisms. This process
387 partially counteracted vegetation-related WY losses in transitional climates like
388 northeastern China, where competing drivers created complex ecohydrological
389 interactions (Fig. 5d-f).

390 Fig. 6 illustrated the spatial distribution of WY trend drivers over the past four
391 decades. Climate change was the dominant factor of WY variation in more than 70%
392 regions, mainly in the Northwest, Southwest, Southeast, Pearl River basins, and other
393 parts of the Yangtze and Yellow River basins. Vegetation changes ranked as the
394 secondary control, dominating WY changes in parts of the Yangtze, Yellow, Songhua,



395 Liao, and Hai Rivers. Remarkably, it was shown that the region where vegetation and
396 $[CO_2]$ had the dominant influence mainly distributes within precipitation ranges of 400–
397 1600 mm. CO_2 -induced effects were least influential at a national scale. This three-
398 tiered hierarchy—climate changes as the primary forcing, vegetation changes as the
399 secondary control, and $[CO_2]$ effects as a localized modifier—reveals how hydrological
400 regimes govern the spatial succession of dominant drivers across China's diverse
401 ecohydrological gradients.



402
403 **Figure 6.** Spatial distributions of dominant factors controlling WY change. Driving factors
404 include climate, vegetation, and $[CO_2]$. Climate: Areas where climate (e.g., precipitation,
405 temperature) is the dominant factor influencing WY change; CO_2 : Areas where $[CO_2]$
406 is the primary driver of WY change; Vegetation: Areas where vegetation changes (e.g.,
407 NDVI, LULC) primarily drive WY changes. Climate-Vegetation: Areas where both climate
408 and vegetation jointly influence WY; Climate- CO_2 : Areas where both climate and $[CO_2]$ jointly
409 contribute to WY change; Vegetation- CO_2 : Areas where vegetation changes and $[CO_2]$ jointly
410 control WY; Climate-Vegetation- CO_2 : Areas where the combined effect of climate, vegetation,
411 and $[CO_2]$ jointly controls WY change. Additionally, the approximate isohyetal line shown in
412 the figure were derived based on annual precipitation data from 1982 to 2017.



3.4 Elasticity of WY to main variables

The sensitivity of WY to precipitation (ϵ_P), NDVI (ϵ_{NDVI}), and $[CO_2]$ (ϵ_{CO_2}) exhibits distinct spatial patterns in (Fig. 7). Nationally averaged elasticity coefficients showed that a 10% increase in precipitation, $[CO_2]$, and NDVI altered WY by 15.5% ($\epsilon_P=1.55$), 5.5% ($\epsilon_{CO_2}=0.55$), and -4.4% ($\epsilon_{NDVI}=-0.44$), respectively, indicating that, in terms of the sensitivity of runoff to changes in each factor, the ranking was precipitation > $[CO_2]$ > NDVI.

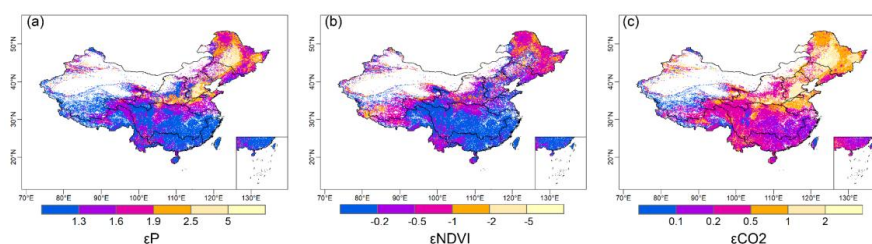


Figure 7. Spatial distribution of elasticity coefficients of WY relative to changes in hydrological variables such as (a) annual precipitation, (b) NDVI, and (c) $[CO_2]$.

The elasticity coefficients of precipitation (ϵ_P), $[CO_2]$ (ϵ_{CO_2}), and vegetation ($|\epsilon_{NDVI}|$) all exhibited a coherent latitudinal decline across China's river basins, showing systematically higher sensitivity in northern regions than southern counterparts. Quantitatively, ϵ_P decreased from 2.09 in the Songhua River basin to 1.15 in the Southeastern Basin, accompanied by similar reductions in $|\epsilon_{NDVI}|$ (from 0.76 to 0.13) and ϵ_{CO_2} (from 1.08 to 0.16) (Table 3).

A distinct abrupt transition zone in elasticity coefficients was identified around 33°N, closely aligning with China's traditional North-South physiographic divide. Around the zone, elasticity coefficients exhibited an abrupt decline from the Yellow River Basin to the Yangtze River Basin. Specifically, the Yellow River Basin showed higher sensitivities to precipitation ($\epsilon_P=1.87$), $[CO_2]$ ($\epsilon_{CO_2}=0.86$), and NDVI ($\epsilon_{NDVI}=-0.53$), which were approximately 1.4, 2.8, and 2.8 times greater, respectively, than those in the Yangtze River Basin ($\epsilon_P=1.31$, $\epsilon_{CO_2}=0.31$, $\epsilon_{NDVI}=-0.19$).



Table 3. Elasticity Coefficients of Runoff to Precipitation, NDVI, and CO₂ in Different Watersheds

Dataset	ϵ_P	ϵ_{NDVI}	ϵ_{CO_2}
Songhua River basin	2.09	-0.76	1.08
Hai River basin	2.13	-0.44	1.12
Yellow River basin	1.87	-0.53	0.86
Yangtze River Basin	1.31	-0.19	0.31
Huai River basin	1.64	-0.18	0.63
Pearl River basin	1.25	-0.17	0.25
Southeast Rivers	1.15	-0.13	0.15

Note: Some LULC types were excluded from the analysis. Due to many missing data points, the Liao River, Southwest, and Northwest river basins were also omitted.

4 Discussion

4.1 Strength of the attribution analysis framework

To address limitations in current methods for analysing the effects of climate, vegetation, and [CO₂] on runoff changes, we developed an attribution analysis framework based on the improved CCW model. This framework has been improved in three aspects. Firstly, the explicit and mechanistic integration of vegetation dynamics and [CO₂] effects overcomes the oversimplifications inherent in conventional approaches. Traditional Budyko-based frameworks often attribute vegetation effects to temporal variations in the parameter "n" by either statistically regressing "n" against vegetation proxies such as NDVI (Liu et al., 2024; Tan et al., 2023) or simplistically equating "n" to vegetation effects (Li et al., 2020b; Zhou et al., 2023). Such approaches conflate structural vegetation changes (e.g., leaf area index) with physiological adjustments (e.g., CO₂-induced stomatal closure), thereby obscuring the independent roles of vegetation dynamics and [CO₂]. For example, while rising [CO₂] levels directly reduce stomatal conductance and transpiration, Budyko-based studies often misinterpret this effect as part of the "n" parameter's variability, erroneously attributing it to vegetation changes (Zeng et al., 2020). In contrast, our framework mechanistically separates these pathways: structural modifications are distinguished from CO₂-driven



458 stomatal physiological responses, resolving contradictions in prior findings where
459 vegetation greening was reported to both mitigate (Zeng et al., 2018) and exacerbate
460 (Farley et al., 2005) runoff changes.

461 Secondly, unlike Budyko-based methods that indirectly represent $[\text{CO}_2]$ impacts
462 through adjustments to potential evapotranspiration (PET)—a practice conflating $[\text{CO}_2]$
463 effects with meteorological drivers like radiation and wind—our framework explicitly
464 quantifies CO_2 's physiological influence on actual evapotranspiration (AET) by
465 mechanistically modeling its role in stomatal conductance and water-use efficiency
466 (WUE). Elevated $[\text{CO}_2]$ reduces stomatal aperture, directly suppressing transpiration
467 while enhancing carbon assimilation. For example, our results show that reduction in
468 transpiration due to CO_2 -driven stomatal closure offsets water losses, a mechanism
469 entirely masked in Budyko frameworks where $[\text{CO}_2]$ effects are ambiguously
470 embedded in PET adjustments or erroneously attributed to vegetation structural
471 changes via the "n" parameter (Liu et al., 2024).

472 Thirdly, while numerous studies have conducted runoff attribution analysis at the
473 basin scale (Liu et al., 2024, 2017; Yang et al., 2022), our grid-scale approach
474 transcends the spatial constraints of fixed watershed boundaries by resolving regional
475 heterogeneity in hydrological drivers. Conventional basin-aggregated methods obscure
476 critical intra-basin differences—for instance, our analysis reveals that grids in the upper
477 Yangtze River basin, where precipitation change dominates runoff trends, necessitate
478 climate scenario-based water resource planning. In contrast, mid-basin grids with
479 significant NDVI-driven greening exhibit pronounced WY reductions, highlighting the
480 need for vegetation management strategies that restrict excessive afforestation in water-
481 sensitive areas (Sun et al., 2022; Yang et al., 2021). By decoupling analysis from rigid
482 watershed boundaries, our framework enables targeted strategies such as restricting
483 reforestation in water-stressed grids or selecting CO_2 -adapted vegetation species,
484 thereby aligning management actions with localized climate-vegetation-hydrology
485 interactions.



486 **4.2 New insights into attribution analysis**

487 Our findings highlighted climate change as the dominant driver of water yield (WY)
488 changes (contributing >70%), consistent with other assessments (Table 4), yet reveal
489 critical regional divergences. Climate impacts dominated in the Northwest and
490 Southwest River Basins, as well as parts of the Yangtze, Yellow, Southeast, and Pearl
491 River Basins, while vegetation and [CO₂] effects prevailed in central China (parts of
492 the Yangtze, Yellow, Songhua, Liao, and Hai River basin)—a spatial pattern slightly
493 distinct from earlier studies. Although previous studies identified human activities as
494 the primary driver in some northern basins (Liao, Hai, and Yellow River Basins) (Yang
495 et al., 2022), their long-term study (1965-2018) diluted the gradually strengthening
496 vegetation signals after 2000 mentioned in other studies (Liu et al., 2017; Sun et al.,
497 2023) through time-averaging. Our findings now confirm the emerging importance of
498 vegetation dynamics in southern basins like the Yangtze through our symmetric 1982-
499 2017 study period.

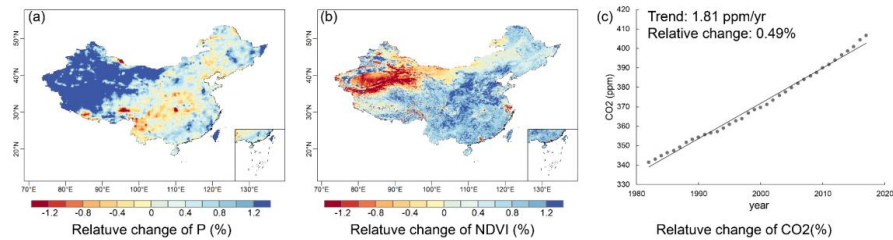
500 **Table 4.** Comparative studies of the contribution of climate variability and vegetation to runoff
501 changes.

Reference	Study region	Study period	Method/Model	Driving factors
(Wei et al., 2024)	Global	1981-2020	Trendy phase 11 +ROF	Climate change
(Liu et al., 2024)	Global	1984-2010; 2000-2100	Improved Budyko	Precipitation
(Zhou et al., 2023)	Global	1850-2014; 2015-2100	Improved Budyko + CMIP6	Land surface changes
(Tan et al., 2023)	Global	2003-2016; 1982-2016	Improved Budyko	Effective precipitation
(Yang et al., 2022)	China	1965-2018	Budyko	P: Northwest river basin, Southwest river basin, Yangtze river basin, Southeast river basin, and Pearl river basin; n: Liaohe river basin, Haihe river basin, Yellow river Basin, Songhuajiang river basin, and Huaihe river basin
(Zhang et al., 2022c)	Yangtze River	2001-2018	CCW Model	Climate variability
(Chen et al., 2022)	Six river basins in China	1982-2015	Gray Relational Analysis (GRA)	Precipitation



(Zhai and Tao, 2021)	China	1982-2015	VIC Model	Climate change
(Li et al., 2020a)	Yihe River	1960-2013	SWAT+WRF	Climate variability
(Shen et al., 2017)	China	1960-2010	Budyko	Underlying surface change (n): the Songhua Basin, the Liaohe Basin and the Haihe Basin; Climate change: in other basins.

502 Elasticity analysis (Section 3.4) revealed distinct sensitivities of WY to
503 environmental drivers: precipitation exhibited the highest elasticity coefficient for the
504 whole China ($\epsilon_P = 1.55$), followed by CO_2 ($\epsilon_{\text{CO}_2} = 0.55$) and NDVI ($\epsilon_{\text{NDVI}} = -0.44$).
505 However, spatial analysis showed that vegetation and $[\text{CO}_2]$ collectively dominated
506 WY changes in 400–1600 mm/yr precipitation zones, despite their lower sensitivity
507 rankings. This apparent contradiction stemmed from the interplay between elasticity
508 and the magnitude of driver change. In the 400–1600 mm/yr precipitation zones, NDVI
509 displayed high spatial heterogeneity (Fig. 8), whereas precipitation fluctuated within a
510 narrower relative range. Consequently, vegetation’s stronger spatiotemporal variability
511 amplified its hydrological influence, overriding its lower elasticity. Similarly, CO_2 ’s
512 historical impact was constrained by its slow accumulation rate (0.49%/yr), yet its
513 relatively high elasticity positions it as a latent driver.



514
515 **Figure 8.** Spatial distribution of relative changes of different variables: (a) annual precipitation,
516 and (b) NDVI.

517 This historical constraint, however, belied CO_2 ’s transformative potential under
518 intensified forcing scenarios. CMIP6 SSP585 projections indicate $[\text{CO}_2]$ will rise at
519 2.34%/yr—nearly fivefold faster than historical rates (Cheng et al., 2022). At this
520 trajectory, CO_2 ’s elasticity would drive a +1.29% annual WY increase, eclipsing both
521 vegetation greening effects and even surpassing precipitation-driven changes in some



522 regions. Such reversal underscores the imperative to prioritize $[\text{CO}_2]$ in long-term water
523 management, particularly in 400–1600 mm/yr precipitation zones.

524 **4.3 Uncertainty in attribution analysis**

525 This study provides valuable insights into the relationship between water resources
526 management and environmental changes, which can guide environmental management
527 strategies. However, several limitations exist that need to be addressed in future work
528 to improve the accuracy and robustness of the results.

529 Firstly, the improved CCW model does not account for the variation and specific
530 values of f_i , assuming f_i is 0. In reality, f_i represents the ratio of interception evaporation
531 to total evaporation, and in regions with abundant vegetation, f_i is not zero. Despite this,
532 considering the small change of f_i in the current year (Zhao et al., 2022), its influence
533 on runoff trends is negligible in our study (Cheng et al., 2017). However, future work
534 should prioritize its calculation to improve the precision of WY estimates.

535 Secondly, the complex interrelationships among climate, vegetation, and $[\text{CO}_2]$
536 cannot be fully disentangled. Vegetation exhibits tight biophysical interactions and
537 feedback with climate, making it difficult to separate the impacts of climate change,
538 vegetation dynamics, and $[\text{CO}_2]$ on hydrological responses. Changes in vegetation,
539 such as NDVI, reflect a combination of climate change, human activities (e.g.,
540 reforestation and irrigation), and natural vegetation growth. Additionally, vegetation
541 greening in upwind regions can increase atmospheric moisture, potentially enhancing
542 precipitation downwind (Zhang et al., 2021a), which may counteract some of the
543 negative impacts of increased evapotranspiration on local WY. Although the climate
544 data used in our model may implicitly capture some of these feedbacks, they cannot be
545 explicitly separated in this analysis. Consequently, our results represent an attempt to
546 estimate the direct first-order net impacts of climate, vegetation greening, and $[\text{CO}_2]$
547 increase on WY (Zhang et al., 2021b). Future research should adopt more



548 comprehensive models that consider soil-vegetation-atmosphere interactions to better
549 differentiate the contributions of each driving factor to WY.

550 Thirdly, the improved CCW model does not incorporate certain human activities,
551 such as dam construction and water extraction, which should be incorporated in future
552 studies. Our research also excludes water bodies and built-up land. While urbanization
553 can increase flood risks due to the growing proportion of impervious surfaces (Wasko
554 and Sharma, 2017), these land-use changes represent a small portion of China's land
555 area.

556 Finally, the future impact of vegetation greening on hydrological dynamics will
557 depend on projected climate warming and drying trends, the persistence of vegetation
558 greening, [CO₂] changes, and the complex feedbacks between climate, soil, and
559 vegetation. These interactions require long-term study, and future research will involve
560 more extensive monitoring to better capture these evolving dynamics.

561 **5 Conclusions**

562 In this study, we improved the CCW model incorporating dynamic water use
563 efficiency (WUE) calculation to explicitly represent CO₂-physiological feedback on
564 water yield. This mechanistic improvement enabled comprehensive national-scale
565 assessment quantifying the relative contributions of climate forcing, vegetation
566 structural changes, and CO₂-driven stomatal regulation to water yield (WY) dynamics
567 in China. The main conclusions are as follows:

568 The improved CCW model effectively simulated WY variations in most basins
569 under increased [CO₂] scenarios, demonstrating its applicability and reliability in
570 modeling WY changes.

571 Climate change, particularly variations in precipitation, emerged as the primary
572 driver influencing WY, displaying significant regional disparities in its effects.
573 Vegetation changes constituted the second most critical factor, predominantly resulting



574 in WY reduction, notably in central China. While the effect of CO₂-induced stomatal
575 closure on WY was comparatively minor. Spatial analysis aligned with isohyetal lines
576 further revealed that vegetation change and [CO₂] exerted greater influence within the
577 400–1600 mm precipitation range.

578 The elasticity analysis of WY indicated that northern basins exhibit higher
579 sensitivity to influencing factors, whereas southern basins demonstrate relatively lower
580 elasticity. Specifically, the absolute elasticity coefficients for the whole China were
581 ranked in descending order as follows: precipitation > [CO₂] > NDVI. Thus,
582 accelerating [CO₂] rise (2.34% /yr under SSP585) will amplify its hydrological role,
583 potentially elevating CO₂-driven WY increases to +1.29% annually by 2100, surpassing
584 climate and vegetation impacts.

585 These insights provide a nuanced understanding of regional hydrological
586 responses, essential for sustainable water resource management under changing
587 environmental conditions.

588 **Acknowledgements**

589 This research was supported by the China National Key R&D Program (grant no.
590 2024YFF1306901).

591 **Data Availability Statement**

592 Datasets used for driving models were obtained from different sources described
593 in Table 1. All the data related to our results in this study can be found online: the NDVI
594 data (<https://doi.org/10.6084/m9.figshare.c.7002225.v1>); the climate data
595 (<https://www.tcdc.ac.cn/zh-hans/data/8028b944-daaa-4511-8769-965612652c49/>); the
596 land use and land cover (LULC) data (<https://zenodo.org/records/8239305>) (Liu et al.,
597 2023); and the [CO₂] (<http://cdiac.esd.ornl.gov/ftp/trends/co2/maunaloa.co2>), except
598 for the streamflow records for hydrological gauging stations, which are available upon
599 reasonable request.



600 **Author contributions**

601 HS designed the study, developed the model code, did the simulation experiments,
602 and wrote the first draft of the paper. HY designed the research and edited the
603 manuscript. CL provided feedback on the results and edited the manuscript.

604 **Competing interests**

605 The contact author has declared that neither they nor their co-authors have any
606 competing interests.

607



Reference

- Adams, M. A., Buckley, T. N., and Turnbull, T. L.: Diminishing CO₂-driven gains in water-use efficiency of global forests, *Nat. Clim. Chang.*, 10, 466–471, <https://doi.org/10.1038/s41558-020-0747-7>, 2020.
- Ban, Z., Xin, C., Fang, Y., Ma, X., Li, D., and Lettenmaier, D. P.: Snowmelt-Radiation Feedback Impact on Western U.S. Streamflow, *Geophysical Research Letters*, 50, e2023GL105118, <https://doi.org/10.1029/2023GL105118>, 2023.
- Chen, C., Park, T., Wang, X., Piao, S., Xu, B., Chaturvedi, R. K., Fuchs, R., Brovkin, V., Ciais, P., Fensholt, R., Tømmervik, H., Bala, G., Zhu, Z., Nemani, R. R., and Myneni, R. B.: China and India lead in greening of the world through land-use management, *Nat Sustain*, 2, 122–129, <https://doi.org/10.1038/s41893-019-0220-7>, 2019.
- Chen, S., Fu, Y. H., Geng, X., Hao, Z., Tang, J., Zhang, X., Xu, Z., and Hao, F.: Influences of Shifted Vegetation Phenology on Runoff Across a Hydroclimatic Gradient, *Front. Plant Sci.*, 12, 802664, <https://doi.org/10.3389/fpls.2021.802664>, 2022.
- Cheng, L., Zhang, L., Wang, Y.-P., Canadell, J. G., Chiew, F. H. S., Beringer, J., Li, L., Miralles, D. G., Piao, S., and Zhang, Y.: Recent increases in terrestrial carbon uptake at little cost to the water cycle, *Nat Commun*, 8, 110, <https://doi.org/10.1038/s41467-017-00114-5>, 2017.
- Cheng, W., Dan, L., Deng, X., Feng, J., Wang, Y., Peng, J., Tian, J., Qi, W., Liu, Z., Zheng, X., Zhou, D., Jiang, S., Zhao, H., and Wang, X.: Global monthly gridded atmospheric carbon dioxide concentrations under the historical and future scenarios, *Sci Data*, 9, 83, <https://doi.org/10.1038/s41597-022-01196-7>, 2022.
- Farley, K. A., Jobbágy, E. G., and Jackson, R. B.: Effects of afforestation on water yield: a global synthesis with implications for policy, *Global Change Biology*, 11, 1565–1576, <https://doi.org/10.1111/j.1365-2486.2005.01011.x>, 2005.
- Fu, J., Liu, B., Wang, W., and Fei, E. X.: Evaluating main drivers of runoff changes across China from 1956 to 2000 by using different budyko-based elasticity methods, *Journal of Environmental Management*, 329, 117070, <https://doi.org/10.1016/j.jenvman.2022.117070>, 2023.
- Gan, G., Liu, Y., and Sun, G.: Understanding interactions among climate, water, and vegetation with the Budyko framework, *Earth-Science Reviews*, 212, 103451, <https://doi.org/10.1016/j.earscirev.2020.103451>, 2021.
- Gutman, G. and Ignatov, A.: The derivation of the green vegetation fraction from NOAA/AVHRR data for use in numerical weather prediction models, *International*



- 643 Journal of Remote Sensing, 19, 1533–1543, <https://doi.org/10.1080/014311698215333>,
644 1998.
- 645 He, J., Yang, K., Tang, W., Lu, H., Qin, J., Chen, Y., and Li, X.: The first high-
646 resolution meteorological forcing dataset for land process studies over China, Sci Data,
647 7, 25, <https://doi.org/10.1038/s41597-020-0369-y>, 2020.
- 648 Hoek Van Dijke, A. J., Herold, M., Mallick, K., Benedict, I., Machwitz, M., Schlerf,
649 M., Pranindita, A., Theeuwes, J. J. E., Bastin, J.-F., and Teuling, A. J.: Shifts in regional
650 water availability due to global tree restoration, Nat. Geosci., 15, 363–368,
651 <https://doi.org/10.1038/s41561-022-00935-0>, 2022.
- 652 Howell, T. A. and Dusek, D. A.: Comparison of Vapor-Pressure-Deficit Calculation
653 Methods—Southern High Plains, J. Irrig. Drain Eng., 121, 191–198,
654 [https://doi.org/10.1061/\(ASCE\)0733-9437\(1995\)121:2\(191\)](https://doi.org/10.1061/(ASCE)0733-9437(1995)121:2(191)), 1995.
- 655 Jiao, Y., Lei, H., Yang, D., Huang, M., Liu, D., and Yuan, X.: Impact of vegetation
656 dynamics on hydrological processes in a semi-arid basin by using a land surface-
657 hydrology coupled model, Journal of Hydrology, 551, 116–131,
658 <https://doi.org/10.1016/j.jhydrol.2017.05.060>, 2017.
- 659 Li, B., Shi, X., Lian, L., Chen, Y., Chen, Z., and Sun, X.: Quantifying the effects of
660 climate variability, direct and indirect land use change, and human activities on runoff,
661 Journal of Hydrology, 584, 124684, <https://doi.org/10.1016/j.jhydrol.2020.124684>,
662 2020a.
- 663 Li, F., Xiao, J., Chen, J., Ballantyne, A., Jin, K., Li, B., Abraha, M., and John, R.: Global
664 water use efficiency saturation due to increased vapor pressure deficit, Science, 381,
665 672–677, <https://doi.org/10.1126/science.adf5041>, 2023.
- 666 Li, H., Shi, C., Zhang, Y., Ning, T., Sun, P., Liu, X., Ma, X., Liu, W., and Collins, A.
667 L.: Using the Budyko hypothesis for detecting and attributing changes in runoff to
668 climate and vegetation change in the soft sandstone area of the middle Yellow River
669 basin, China, Science of The Total Environment, 703, 135588,
670 <https://doi.org/10.1016/j.scitotenv.2019.135588>, 2020b.
- 671 Li, H., Cao, Y., Xiao, J., Yuan, Z., Hao, Z., Bai, X., Wu, Y., and Liu, Y.: A daily gap-
672 free normalized difference vegetation index dataset from 1981 to 2023 in China, Sci
673 Data, 11, 527, <https://doi.org/10.1038/s41597-024-03364-3>, 2024a.
- 674 Li, M., Li, C., Jiang, Z., Zhang, X., and Zwiers, F. W.: Deciphering China’s Complex
675 Pattern of Summer Precipitation Trends, Earth’s Future, 10, e2022EF002797,
676 <https://doi.org/10.1029/2022EF002797>, 2022.



- 677 Li, X., Xu, X., Sonnenborg, T. O., Andreasen, M., and He, C.: Effect of ecological
678 restoration on evapotranspiration and water yield in the agro-pastoral ecotone in
679 northern China during 2000–2018, *Journal of Hydrology*, 638, 131531,
680 <https://doi.org/10.1016/j.jhydrol.2024.131531>, 2024b.
- 681 Liang, L., Han, Z., Chen, W., Li, J., Liang, M., and Shen, S.: The source, transport,
682 deposition and direct radiative effect of mineral dust over western China: A modeling
683 study of July 2022 with focus on the Tibetan Plateau, *Atmospheric Research*, 311,
684 107708, <https://doi.org/10.1016/j.atmosres.2024.107708>, 2024.
- 685 Liu, C., Feng, S., Zhang, Q., Hu, J., Ma, N., Ci, H., Kong, D., and Gu, X.: Critical
686 influence of vegetation response to rising CO₂ on runoff changes, *Science of The Total
687 Environment*, 906, 167717, <https://doi.org/10.1016/j.scitotenv.2023.167717>, 2024.
- 688 Liu, J., Zhang, Q., Singh, V. P., and Shi, P.: Contribution of multiple climatic variables
689 and human activities to streamflow changes across China, *Journal of Hydrology*, 545,
690 145–162, <https://doi.org/10.1016/j.jhydrol.2016.12.016>, 2017.
- 691 Ma, C., Yao, J., Mo, Y., Zhou, G., Xu, Y., and He, X.: Prediction of summer
692 precipitation via machine learning with key climate variables: A case study in
693 Xinjiang, China, *Journal of Hydrology: Regional Studies*, 56, 101964,
694 <https://doi.org/10.1016/j.ejrh.2024.101964>, 2024.
- 695 Ma, T., Wang, T., Yang, D., and Yang, S.: Impacts of vegetation restoration on water
696 resources and carbon sequestration in the mountainous area of Haihe River basin, China,
697 *Science of The Total Environment*, 869, 161724,
698 <https://doi.org/10.1016/j.scitotenv.2023.161724>, 2023.
- 699 Mu, S., Zhou, S., Chen, Y., Li, J., Ju, W., and Odeh, I. O. A.: Assessing the impact of
700 restoration-induced land conversion and management alternatives on net primary
701 productivity in Inner Mongolian grassland, China, *Global and Planetary Change*, 108,
702 29–41, <https://doi.org/10.1016/j.gloplacha.2013.06.007>, 2013.
- 703 Ogotu, B. O., D’Adamo, F., and Dash, J.: Impact of vegetation greening on carbon and
704 water cycle in the African Sahel-Sudano-Guinean region, *Global and Planetary Change*,
705 202, 103524, <https://doi.org/10.1016/j.gloplacha.2021.103524>, 2021.
- 706 Peng, H., Tague, C., and Jia, Y.: Evaluating the eco-hydrologic impacts of reforestation
707 in the Loess Plateau, China, using an eco-hydrologic model, *Ecohydrology*, 9, 498–513,
708 <https://doi.org/10.1002/eco.1652>, 2016.
- 709 Running, S. W., Thornton, P. E., Nemani, R., and Glassy, J. M.: Global Terrestrial
710 Gross and Net Primary Productivity from the Earth Observing System, in: *Methods in
711 Ecosystem Science*, edited by: Sala, O. E., Jackson, R. B., Mooney, H. A., and Howarth,



- 712 R. W., Springer New York, New York, NY, 44–57, [https://doi.org/10.1007/978-1-](https://doi.org/10.1007/978-1-4612-1224-9_4)
713 4612-1224-9_4, 2000.
- 714 Saltelli, A., Ratto, M., Andres, T., Campolongo, F., Cariboni, J., Gatelli, D., Saisana,
715 M., and Tarantola, S.: Global Sensitivity Analysis. The Primer, 1st ed., Wiley,
716 <https://doi.org/10.1002/9780470725184>, 2007.
- 717 Shen, Q., Cong, Z., and Lei, H.: Evaluating the impact of climate and underlying
718 surface change on runoff within the Budyko framework: A study across 224 catchments
719 in China, *Journal of Hydrology*, 554, 251–262,
720 <https://doi.org/10.1016/j.jhydrol.2017.09.023>, 2017.
- 721 Shi, S., Wang, P., and Yu, J.: Vegetation greening and climate change promote an
722 increase in evapotranspiration across Siberia, *Journal of Hydrology*, 610, 127965,
723 <https://doi.org/10.1016/j.jhydrol.2022.127965>, 2022.
- 724 Sims, D. A., Rahman, A. F., Cordova, V. D., Baldocchi, D. D., Flanagan, L. B.,
725 Goldstein, A. H., Hollinger, D. Y., Misson, L., Monson, R. K., Schmid, H. P., Wofsy,
726 S. C., and Xu, L.: Midday values of gross CO₂ flux and light use efficiency during
727 satellite overpasses can be used to directly estimate eight-day mean flux, *Agricultural*
728 *and Forest Meteorology*, 131, 1–12, <https://doi.org/10.1016/j.agrformet.2005.04.006>,
729 2005.
- 730 Sun, W., Ding, X., Su, J., Mu, X., Zhang, Y., Gao, P., and Zhao, G.: Land use and cover
731 changes on the Loess Plateau: A comparison of six global or national land use and cover
732 datasets, *Land Use Policy*, 119, 106165,
733 <https://doi.org/10.1016/j.landusepol.2022.106165>, 2022.
- 734 Sun, X., Dong, Q., and Zhang, X.: Attribution analysis of runoff change based on
735 Budyko-type model with time-varying parameters for the Lhasa River Basin, Qinghai–
736 Tibet Plateau, *Journal of Hydrology: Regional Studies*, 48, 101469,
737 <https://doi.org/10.1016/j.ejrh.2023.101469>, 2023.
- 738 Tan, X., Tan, X., Liu, B., and Huang, Z.: Contribution of changes in vegetation
739 composition and climate variability on streamflow across the global watersheds,
740 *CATENA*, 232, 107394, <https://doi.org/10.1016/j.catena.2023.107394>, 2023.
- 741 Tan, X., Jia, Y., Yang, D., Niu, C., and Hao, C.: Impact ways and their contributions to
742 vegetation-induced runoff changes in the Loess Plateau, *Journal of Hydrology:*
743 *Regional Studies*, 51, 101630, <https://doi.org/10.1016/j.ejrh.2023.101630>, 2024.
- 744 Wang, Y., Wang, S., Wang, C., and Zhao, W.: Runoff sensitivity increases with land
745 use/cover change contributing to runoff decline across the middle reaches of the Yellow
746 River basin, *Journal of Hydrology*, 600, 126536,
747 <https://doi.org/10.1016/j.jhydrol.2021.126536>, 2021.



- 748 Wasko, C. and Sharma, A.: Global assessment of flood and storm extremes with
749 increased temperatures, *Sci Rep*, 7, 7945, <https://doi.org/10.1038/s41598-017-08481-1>,
750 2017.
- 751 Wei, H., Zhang, Y., Huang, Q., Chiew, F. H. S., Luan, J., Xia, J., and Liu, C.: Direct
752 vegetation response to recent CO₂ rise shows limited effect on global streamflow, *Nat*
753 *Commun*, 15, 9423, <https://doi.org/10.1038/s41467-024-53879-x>, 2024.
- 754 Xu, X., Yang, D., Yang, H., and Lei, H.: Attribution analysis based on the Budyko
755 hypothesis for detecting the dominant cause of runoff decline in Haihe basin, *Journal*
756 *of Hydrology*, 510, 530–540, <https://doi.org/10.1016/j.jhydrol.2013.12.052>, 2014.
- 757 Xue, B., A, Y., Wang, G., Helman, D., Sun, G., Tao, S., Liu, T., Yan, D., Zhao, T.,
758 Zhang, H., Chen, L., Sun, W., and Xiao, J.: Divergent Hydrological Responses to Forest
759 Expansion in Dry and Wet Basins of China: Implications for Future Afforestation
760 Planning, *Water Resources Research*, 58, e2021WR031856,
761 <https://doi.org/10.1029/2021WR031856>, 2022.
- 762 Yang, H. and Yang, D.: Derivation of climate elasticity of runoff to assess the effects
763 of climate change on annual runoff: DERIVATION OF CLIMATE ELASTICITY OF
764 RUNOFF, *Water Resour. Res.*, 47, <https://doi.org/10.1029/2010WR009287>, 2011.
- 765 Yang, H. and Yang, D.: Climatic factors influencing changing pan evaporation across
766 China from 1961 to 2001, *Journal of Hydrology*, 414–415, 184–193,
767 <https://doi.org/10.1016/j.jhydrol.2011.10.043>, 2012.
- 768 Yang, H., Xiong, L., Xiong, B., Zhang, Q., and Xu, C.-Y.: Separating runoff change by
769 the improved Budyko complementary relationship considering effects of both climate
770 change and human activities on basin characteristics, *Journal of Hydrology*, 591,
771 125330, <https://doi.org/10.1016/j.jhydrol.2020.125330>, 2020.
- 772 Yang, H., Xu, H., Huntingford, C., Ciais, P., and Piao, S.: Strong direct and indirect
773 influences of climate change on water yield confirmed by the Budyko framework,
774 *Geography and Sustainability*, 2, 281–287,
775 <https://doi.org/10.1016/j.geosus.2021.11.001>, 2021.
- 776 Yang, L., Zhao, G., Tian, P., Mu, X., Tian, X., Feng, J., and Bai, Y.: Runoff changes in
777 the major river basins of China and their responses to potential driving forces, *Journal*
778 *of Hydrology*, 607, 127536, <https://doi.org/10.1016/j.jhydrol.2022.127536>, 2022.
- 779 Yang, Y., Xiao, P., Feng, X., and Li, H.: Accuracy assessment of seven global land
780 cover datasets over China, *ISPRS Journal of Photogrammetry and Remote Sensing*, 125,
781 156–173, <https://doi.org/10.1016/j.isprsjprs.2017.01.016>, 2017.



- 782 Yang, Y., Roderick, M. L., Zhang, S., McVicar, T. R., and Donohue, R. J.: Hydrologic
783 implications of vegetation response to elevated CO₂ in climate projections, *Nature*
784 *Clim Change*, 9, 44–48, <https://doi.org/10.1038/s41558-018-0361-0>, 2019.
- 785 Yang, Y., Roderick, M. L., Guo, H., Miralles, D. G., Zhang, L., Fatichi, S., Luo, X.,
786 Zhang, Y., McVicar, T. R., Tu, Z., Keenan, T. F., Fisher, J. B., Gan, R., Zhang, X., Piao,
787 S., Zhang, B., and Yang, D.: Evapotranspiration on a greening Earth, *Nat Rev Earth*
788 *Environ*, 4, 626–641, <https://doi.org/10.1038/s43017-023-00464-3>, 2023.
- 789 Zeng, F., Ma, M.-G., Di, D.-R., and Shi, W.-Y.: Separating the Impacts of Climate
790 Change and Human Activities on Runoff: A Review of Method and Application, *Water*,
791 12, 2201, <https://doi.org/10.3390/w12082201>, 2020.
- 792 Zeng, Z., Piao, S., Li, L. Z. X., Wang, T., Ciais, P., Lian, X., Yang, Y., Mao, J., Shi, X.,
793 and Myneni, R. B.: Impact of Earth Greening on the Terrestrial Water Cycle, *J. Climate*,
794 31, 2633–2650, <https://doi.org/10.1175/JCLI-D-17-0236.1>, 2018.
- 795 Zhai, R. and Tao, F.: Contributions of climate change and human activities to runoff
796 change in seven typical catchments across China, *Science of The Total Environment*,
797 605–606, 219–229, <https://doi.org/10.1016/j.scitotenv.2017.06.210>, 2017.
- 798 Zhai, R. and Tao, F.: Climate Change in China Affects Runoff and Terrestrial
799 Ecosystem Water Retention More Than Changes in Leaf Area Index and Land
800 Use/Cover Over the Period 1982–2015, *JGR Biogeosciences*, 126, e2020JG005902,
801 <https://doi.org/10.1029/2020JG005902>, 2021.
- 802 Zhang, B., Tian, L., Zhao, X., and Wu, P.: Feedbacks between vegetation restoration
803 and local precipitation over the Loess Plateau in China, *Sci. China Earth Sci.*, 64, 920–
804 931, <https://doi.org/10.1007/s11430-020-9751-8>, 2021a.
- 805 Zhang, B., Tian, L., Yang, Y., and He, X.: Revegetation Does Not Decrease Water
806 Yield in the Loess Plateau of China, *Geophysical Research Letters*, 49,
807 e2022GL098025, <https://doi.org/10.1029/2022GL098025>, 2022a.
- 808 Zhang C., WU C., KUAI S., PENG Z., Chang R., and ZHANG S.: Water-heat coupling
809 model-based study on runoff driving mechanism of Zhenjiangguan Watershed, *Water*
810 *Resources and Hydropower Engineering*, 53, 78–87,
811 <https://doi.org/10.13928/j.cnki.wrahe.2022.08.008>, 2022b.
- 812 Zhang, J., Zhang, Y., Sun, G., Song, C., Dannenberg, M. P., Li, J., Liu, N., Zhang, K.,
813 Zhang, Q., and Hao, L.: Vegetation greening weakened the capacity of water supply to
814 China’s South-to-North Water Diversion Project, *Hydrol. Earth Syst. Sci.*, 25, 5623–
815 5640, <https://doi.org/10.5194/hess-25-5623-2021>, 2021b.



- 816 Zhang, J., Zhang, Y., Sun, G., Song, C., Li, J., Hao, L., and Liu, N.: Climate Variability
817 Masked Greening Effects on Water Yield in the Yangtze River Basin During 2001–
818 2018, *Water Resources Research*, 58, e2021WR030382,
819 <https://doi.org/10.1029/2021WR030382>, 2022c.
- 820 Zhang, S., Yang, H., Yang, D., and Jayawardena, A. W.: Quantifying the effect of
821 vegetation change on the regional water balance within the Budyko framework,
822 *Geophysical Research Letters*, 43, 1140–1148, <https://doi.org/10.1002/2015GL066952>,
823 2016a.
- 824 Zhang, X., Zhao, T., Xu, H., Liu, W., Wang, J., Chen, X., and Liu, L.: GLC_FCS30D:
825 the first global 30 m land-cover dynamics monitoring product with a fine classification
826 system for the period from 1985 to 2022 generated using dense-time-series Landsat
827 imagery and the continuous change-detection method, *Earth Syst. Sci. Data*, 16, 1353–
828 1381, <https://doi.org/10.5194/essd-16-1353-2024>, 2024.
- 829 Zhang, Y., Song, C., Sun, G., Band, L. E., McNulty, S., Noormets, A., Zhang, Q., and
830 Zhang, Z.: Development of a coupled carbon and water model for estimating global
831 gross primary productivity and evapotranspiration based on eddy flux and remote
832 sensing data, *Agricultural and Forest Meteorology*, 223, 116–131,
833 <https://doi.org/10.1016/j.agrformet.2016.04.003>, 2016b.
- 834 Zhao, F., Wu, Y., Ma, S., Lei, X., and Liao, W.: Increased Water Use Efficiency in
835 China and Its Drivers During 2000–2016, *Ecosystems*, 25, 1476–1492,
836 <https://doi.org/10.1007/s10021-021-00727-4>, 2022.
- 837 Zhou, S., Yu, B., Huang, Y., and Wang, G.: The effect of vapor pressure deficit on
838 water use efficiency at the subdaily time scale, *Geophysical Research Letters*, 41, 5005–
839 5013, <https://doi.org/10.1002/2014GL060741>, 2014.
- 840 Zhou, S., Yu, B., Lintner, B. R., Findell, K. L., and Zhang, Y.: Projected increase in
841 global runoff dominated by land surface changes, *Nat. Clim. Chang.*, 13, 442–449,
842 <https://doi.org/10.1038/s41558-023-01659-8>, 2023.
- 843
844